6

Oxidative dehydrogenation on carbon surfaces

Designing and developing a highly selective catalyst has been an intriguing and challenging goal in catalysis research. The development of novel industrial catalysts ideally begins with the identification of a catalytically active species and an appropriate catalytic support [LePage, 1997]. Experimental studies on the active and passive properties of carbon as a catalyst have indicated that elemental carbon exhibits properties of both an active catalytic species and of a catalytic support [Maximova, 2002; Reshetenko et al., 2004; Serp et al., 2003]. The catalytic properties of carbon, however, is less known as compared to traditional metal-oxide catalysts. In this chapter, I aim at the characterization of the catalytic properties of graphitic carbon surfaces as an active phase for the oxidative dehydrogenation (ODH) of ethylbenzene. The ODH reaction involves the conversion of ethylbenzene to styrene in the presence of oxygen and is one of the top ten industrial processes [Kochloefl, 1997]. Here, the conversion of ethylbenzene to styrene on various pristine and oxidized carbon surfaces is monitored using thermal desorption spectroscopy (TDS). The surface concentrations of the educt (ethylbenzene) and the product (styrene) species are used to evaluate parameters such as catalytic selectivity, percentage conversion etc., of carbon surfaces. This chapter begins with a brief overview of carbon's role in the field of heterogenous catalysis. Later, the desorption kinetics of ethylbenzene from pristine and oxidized carbon surfaces is presented. The ODH reaction mechanism is proposed which is based on comparable traditional organic chemistry reactions. The thermal desorption of ethylbenzene and styrene from highly oriented pyrolytic graphite (HOPG), single-wall carbon nano-

tube (SWNT) bundles, carbon nanofibers (CNFs) and colloidal graphite (CG) are used to obtain the respective desorption parameters and binding energies.

6.1. Carbon in heterogeneous catalysis

Elemental carbon plays a multi-faceted role in the field of heterogenous catalysis. For instance, carbon nanotubes, carbon nanofibers and activated carbon have been used as effective support for metal particles in catalytic conversion of hydrocarbons [Reshetenko et al., 2004; Ros, 2002; Serp et al., 2003]. Likewise, for the oxidation of alcohols, various carbon surfaces have been used to anchor transition metal catalysts [Kua and Goddard III, 1999; Serp et al., 2003]. When compared to conventional supports such as alumina, catalysts embedded in a carbon matrix offer better efficiency even at moderate temperatures. The higher efficiency of carbon substrates as catalyst supports is ascribed to their extremely porous structure. The specific surface area of carbon nanofibers, for instance, is on the order of 100s of $m^2\,g^{-1}$). Parallel to this, they are inert to most active catalytic phases, due to only a weak interaction and also offer high resistance to corrosion [Park et al., 2003; Reshetenko et al., 2004; Ros, 2002; Serp et al., 2003]. In addition to this role as an efficient catalytic support, they can function as active catalyst phases themselves. The use of carbon as an active catalytic phase is possibly first demonstrated in the oxidative dehydrogenation reaction of ethylbenzene. It is the single-most studied catalytic conversion that involves carbon [Muradov, 2001; Schlögl, 1997]. The catalytic activity of graphitic and porous carbon surfaces such as HOPG and CNFs in a heterogenous oxidation reaction is due to the availability of delocalized π-electrons. Also instrumental in this aspect is the high density of reactive edge planes in graphitic carbon materials, which immobilizes activated reactant species that are formed on their surfaces [Sanchez-Cortezon, 2002; Schlögl, 1997].

6.1.1. Oxidative dehydrogenation on carbon surfaces

Of many oxidation reactions catalyzed by carbon the partial oxidation of ethylbenzene has gained increased attention [Drago and Jurczyk, 1994; Guerrero-Ruiz and Rodríguez-Ramoz, 1994; Mestl et al., 2001; Pereira et al., 2000, 2002]. This reaction, known as oxidative dehydrogenation, involves the conversion of ethylbenzene to styrene as represented below:

$$C_6H_5C_2H_5 + \frac{1}{2}O_2 \rightleftharpoons C_6H_5C_2H_3 + H_2O\,, \quad \Delta H^0_{298} = -124.2\,\mathrm{kJ\,mol^{-1}}. \tag{6.1}$$

To a lesser extent, the increased interest, is attributed to the fascination of developing carbon-based model catalytic systems and its extension to industrial level catalysis. However, the dominant reason, is the ambition to develop a novel method

for styrene synthesis, i.e., as an alternative method to the incompetent industrial equivalent. Industrially, the above conversion is achieved by passing a mixture of ethylbenzene and super-heated steam (in the ratio 1:10) over a metal oxide catalyst (typically K-promoted Fe_2O_3) at temperatures roughly around 700 °C [Cavani and Trifirò, 1995; Kochloefl, 1997]. This process, known as non-oxidative dehydrogenation (DH) of ethylbenzene [Eq. (6.2)] accounts for more than 90 % of the industrial styrene production [Kochloefl, 1997]:

$$C_6H_5C_2H_5 \underset{+H_2O\,,-H_2}{\overset{K-\ Fe_2O_3}{\rightleftharpoons}} C_6H_5C_2H_3, \quad \Delta H^0_{298} = +117.5\,\mathrm{kJ\,mol^{-1}}. \tag{6.2}$$

As indicated by the positive standard enthalpy of the reaction, this conversion requires high energy consumption. Also, due to the thermodynamic equilibrium, the maximum conversion of ethylbenzene is limited below 70 %. Lastly, the high steam-to-hydrocarbon (10:1) ratio results in the formation of by-products like benzene and toluene, that limits the yield and purity of the resulting styrene [Cavani and Trifirò, 1995; Geisler et al., 2003]. Oxidative dehydrogenation of ethylbenzene [Eq. (6.1)], on the other hand, occurs at lower temperatures (350–450 °C) and is a highly exothermic reaction, due to water formation. Moreover, the removal of hydrogen (by the formation of water), effectively shifts the equilibrium in Eq. (6.1) to far right, thus allowing conversion up to 85 % [Cavani and Trifirò, 1999].

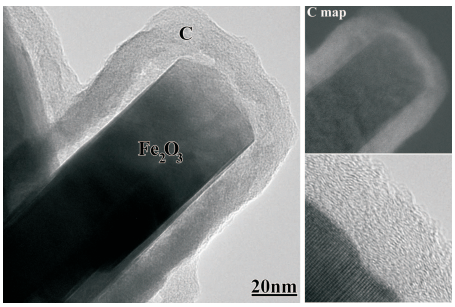

Figure 6.1.: TEM image of carbon deposit (C) formed on Fe_2O_3 crystal during oxidative dehydrogenation. Figure adapted from [Roddatis and Su, 2001].

This combination of favorable factors always has always been a strong incentive for a detailed study of the ODH of ethylbenzene. The application of carbon as the active catalytic phase for ODH is proposed after a mechanistic study revealed the catalytic activity of graphitic deposit formed on the K–Fe phase (Fig. 6.1) [Muhler et al., 1992; Roddatis and Su, 2001]. For example, an induction period attributed to the growth of carbon deposit is observed when ODH of ethylbenzene is conducted in the presence of K-promoted Fe_2O_3 [Mestl et al., 2001]. Subsequently, the catalytic performance of various carbon surfaces for many ODH reactions was explored [Drago and Jurczyk, 1994; Guerrero-Ruiz and Rodríguez-Ramoz, 1994; Maximova, 2002; Mestl et al., 2001; Pereira et al., 2000, 2002]. However, because of the complex polymorphism exhibited by elemental carbon and relatively unknown stoichiometry of carbon surfaces, a clear understanding of the carbon catalysts is limited, when compared to conventional metal-oxide or metal catalysts [Schlögl, 1997]. Nevertheless, their catalytic activity is tentatively assigned to the greater density of active sites, such as edge planes (or prismatic planes) and dangling bonds

(refer chapter 3 for a discussion of their structure) [Ehrburger and Vix-Guterl, 1998; Sanchez-Cortezon, 2002]. Reactive oxygen species—a decisive factor for selective oxidation reactions—can easily be formed and stabilized over basal and edge planes of their graphitic structure [Sanchez-Cortezon, 2002]. Another crucial factor for enhanced catalytic activity of carbon surfaces is the presence of various polyfunctional surface groups (typically carboxylic acid, keto, phenolic groups etc., see Fig. 5.3 in chapter 5) [Boehm, 1994; Ehrburger and Vix-Guterl, 1998; Maximova, 2002; Pereira et al., 1999]. These oxygen carrying species are formed on a carbon surface when they are subjected to oxidation under suitable conditions (see chapter 5 for details on oxidation of carbon surfaces). However, because of this very diverse nature of carbon surfaces, the real mechanism by which they catalyze the ODH reaction is less understood. Identification of the elementary steps of the ODH reaction mechanism is of central importance in order to address the catalytic description of the surface in terms of percentage conversion or selectivity. A recent kinetic study has suggested that ODH involves a bimolecular surface reaction between adsorbed ethylbenzene and oxygen molecules which is the rate determining step [Maximova, 2002]. This mechanism fits into the Langmuir-Hinshelwood (LH) formalism of surface reactions, where the interaction between ethylbenzene and oxygen adsorbed on basal or edge planes of sp^2 carbon plays a decisive role. Apart from the LH mechanism, there have been some suggestions that the reaction proceeds through a two-stepped reaction process known as Mars-van Krevelen (MvK) mechanism. In the following section, both these reaction mechanisms are discussed.

6.1.2. Mechanism of oxidative dehydrogenation of ethylbenzene

Due to many reasons, the precise mechanism of the ODH over the carbon surface remains as a debated topic. For instance, the precise functions of diverse polyfunctional surface groups are not understood as far the reaction mechanism is considered [Schlögl, 1997]. Also, unlike conventional metal oxide catalysts the active centers on carbon surfaces are less understood, for example, in terms of their catalytic activity. Schraut et al. [1987] have addressed the mechanism of ethylbenzene oxidation on a carbon surface by extending a scheme similar to conventional metal oxide catalysis. This mechanism known as Mars-van Krevelen mechanism, proceeds through a two-step reaction [Campbell, 1988]. The elementary steps of MvK mechanism are shown in Eqs. (6.3a)–(6.3d) [Schraut et al., 1987]. The MvK mechanism is initiated by the adsorption of an ethylbenzene molecule on a carbon surface and the subsequent nucleophilic oxidation by a lattice oxygen, L_{ox} [Eqs. (6.3a)–(6.3c)]. The result of this step is the formation of a lattice vacancy, L_{red}. The second step of the mechanism is the rate-determining slow replenishment of the lattice vacancy by gaseous oxygen atoms [Eq. (6.3d)]. Following equations represent elementary steps

in the MvK mechanism:

$$\mathrm{EB} + \mathrm{L_{ox}} \underset{k_{-1}}{\overset{k_1}{\rightleftharpoons}} \mathrm{EB} \cdot \mathrm{L_{ox}}, \tag{6.3a}$$

$$\mathrm{EB} \cdot \mathrm{L_{ox}} \xrightarrow{k_2} \mathrm{ST} \cdot \mathrm{L_{red}}, \tag{6.3b}$$

$$\mathrm{ST} \cdot \mathrm{L_{red}} \underset{k_{-3}}{\overset{k_3}{\rightleftharpoons}} \mathrm{ST} + \mathrm{L_{red}}, \tag{6.3c}$$

$$\mathrm{L_{red}} + \frac{1}{2}\mathrm{O_2} \underset{k_{-4}}{\overset{k_4}{\rightleftharpoons}} \mathrm{L_{ox}} + \mathrm{H_2O}, \tag{6.3d}$$

where EB, $\mathrm{L_{ox}}$ and $\mathrm{L_{red}}$ represent ethylbenzene, a lattice oxide (such as quinone or carbonyl) and a lattice vacancy (for example, hydroquinone) respectively and k_i's and k_{-i}'s are respective rate constants.

However, the extension of the MvK mechanism to describe the catalytic function of carbon has been under dispute due to an entirely different surface chemistry [Maximova, 2002]. For example, conventional metal-oxide catalysts used for selective oxidation formally contain a cation with an empty, half or full outermost *d*-orbital. Typical examples of such cations are $\mathrm{Mo}^{6+}(4d^0)$, $\mathrm{Fe}^{3+}(3d^5)$ or $\mathrm{Sb}^{5+}(4d^{10})$. The oxides of such elements have the ability to release associated lattice oxygen (O^{2-}) for the incorporation into organic adsorbates [Campbell, 1988]. On the contrary, the oxides of elemental carbon are acidic and hence their availability for nucleophilic attack is not feasible [Cotton and Wilkinson, 1980]. Also, many surface adsorbed oxygen species, such as a neutral singlet oxygen (O), superoxide ion ($\mathrm{O_2}^-$), oxygen anion (O^-) or covalently bonded oxygen atom are electrophilic and can readily attack electron rich carbon. The carbon atom of the methylene group ($-\mathrm{CH_2}-$) in an ethylbenzene molecule provides an electron rich environment [i.e., surrounded by electron releasing $-\mathrm{CH_3}$ (methyl) and $-\mathrm{C_6H_5}$ (phenyl) groups on both sides] and hence is susceptible to an attack by the aforementioned reactive oxygen species [Bielański and Haber, 1991; Cornils et al., 2000]. Also, the application of the MvK mechanism assumes a rate-determining adsorption or desorption step [Campbell, 1988]. However, due to the low activation of hydrocarbon molecules on carbon surfaces, the rate of the bimolecular surface reaction, i.e., Eq. (6.3b), is generally smaller compared to the rate of desorption or adsorption. Because of this disparity, it is inaccurate to treat the catalysis on carbon using the MvK mechanism. A better representation of the ODH mechanism on carbon can be made using the Langmuir-Hinshelwood (LH) mechanism [Hinshelwood, 1940]. The sequences of elementary reactions in the LH mechanism involve the steps similar to the Eqs. (6.3a)–(6.3c) in the above reaction scheme. The reaction mechanism involves a fast adsorption of ethylbenzene and oxygen molecules (step 1 in Fig. 6.2), which is followed by a rate-determining slow bimolecular reaction (step 2) between adsorbed oxygen and ethylbenzene [Eq. (6.3b)]. Final step in the mechanism is the desorption of products, styrene and water [Maximova, 2002]. Using the LH mechanism, the complete

description of adsorption-reaction-desorption equilibria would involve the ad- and desorption equilibria for ethylbenzene and styrene as well as the equilibrium between the bimolecular surface reaction between adsorbed ethylbenzene and oxygen. The various equilibria that coexist can then be described by the following set of

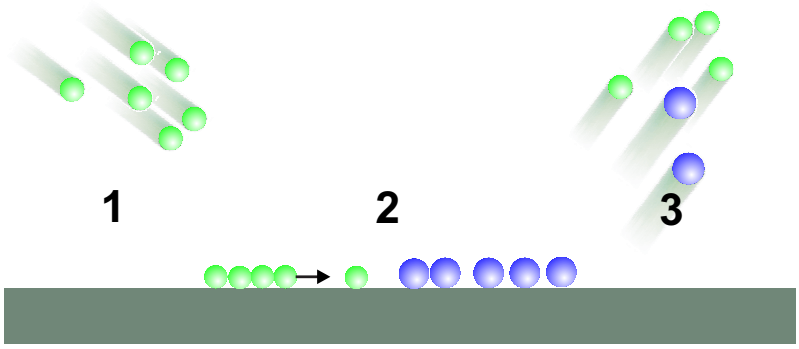

Figure 6.2.: Schematic representation of elementary steps involved in the Langmuir-Hinshelwood mechanism [Campbell, 1988]. Elementary steps involve [1] the adsorption of ethylbenzene (green spheres): Eq. (6.4a), [2] surface reaction between adsorbed oxygen and ethylbenzene molecules: Eq. (6.4b) and [3] desorption of styrene (blue spheres) and water: Eq. (6.4c).

equations:

$$[\mathrm{EB}]_s \underset{k_{-5}}{\overset{k_5}{\rightleftharpoons}} [\mathrm{EB}]_g, \tag{6.4a}$$

$$[\mathrm{EB}]_s + [\mathrm{O}]_s \underset{k_{-6}}{\overset{k_6}{\rightleftharpoons}} [\mathrm{ST}]_s + [\mathrm{H_2O}]_s, \tag{6.4b}$$

$$[\mathrm{ST}]_s \underset{k_{-7}}{\overset{k_7}{\rightleftharpoons}} [\mathrm{ST}]_g, \tag{6.4c}$$

where $[\mathrm{X}]_g$ and $[\mathrm{X}]_s$ represent the gas phase and surface concentrations of reactants and products (X = EB, ST, O and $\mathrm{H_2O}$), while k_i's and k_{-i}'s are respective rate constants for forward and backward reactions. The above three equilibria can be studied as a set of simultaneous [Eqs. (6.4a) and (6.4b)] and consecutive reactions [Eqs. (6.4b) and (6.4c)] of the general type [Laidler, 1987]:

$$\left.\begin{array}{c} [\mathrm{EB}]_s \xrightarrow{k_5} [\mathrm{EB}]_g \\ [\mathrm{EB}]_s \xrightarrow{k_6} [\mathrm{ST}]_s \end{array}\right\} \Rightarrow \text{simultaneous reactions,}$$

$$\left.[\mathrm{EB}]_s \xrightarrow{k_6} [\mathrm{ST}]_s \xrightarrow{k_7} [\mathrm{ST}]_g \right\} \Rightarrow \text{consecutive reactions.}$$

In agreement with the above set of equilibria, the expression for the rate of decrease in surface concentration of ethylbenzene has contributions from two competitive

processes: the rate of desorption of ethylbenzene and the rate at which bimolecular reaction proceeds:

$$-\frac{d[\mathrm{EB}]_s}{dt} = k_5\ [\mathrm{EB}]_s + k_6\ [\mathrm{EB}]_s\ [\mathrm{O}]_s. \tag{6.5}$$

Similarly, the rate of disappearance of styrene from the surface can be written as:

$$-\frac{d[\mathrm{ST}]_s}{dt} = k_7\ [\mathrm{ST}]_s - k_6\ [\mathrm{EB}]_s\ [\mathrm{O}]_s. \tag{6.6}$$

To obtain the activation energy for the conversion of ethylbenzene, both these equations need to be solved. However, in order to calculate the kinetic and thermodynamic parameters related to the desorption, the above set of equations can be approximated by assuming that the rate of desorption is much greater than that for the surface reaction (i.e., $k_5\ [\mathrm{EB}]_s \gg k_6\ [\mathrm{EB}]_s\ [\mathrm{O}]_s$). This assumption is the foundation for treating a surface reaction by the LH mechanism and is explained on the basis of greater activation energies and smaller pre-exponential frequency factors for the surface reactions, when compared to those of desorption [Campbell, 1988; Nørskov and Stolitze, 1997]. Using the above approximation, Eqs. (6.5) and (6.6) can be re-written in the Arrhenius form as:

$$-\frac{d[\mathrm{EB}]_s}{dt} = \nu_{EB}\ [\mathrm{EB}]_s\ \exp(-\Delta E_{EB}/k_B T) \tag{6.7}$$

and

$$-\frac{d[\mathrm{ST}]_s}{dt} = \nu_{ST}\ [\mathrm{ST}]_s\ \exp(-\Delta E_{ST}/k_B T), \tag{6.8}$$

where ν_{EB}, and ν_{ST} are the frequency factors for the desorption of ethylbenzene and styrene, respectively. ΔE_{EB}, and ΔE_{ST} are corresponding activation energies. Eqs. (6.7) and (6.8) are analogous to the rate of the desorption of ethylbenzene and styrene from carbon surfaces, and therefore are used to evaluate the respective TD spectra to obtain the pre-exponential frequency factors and activation energies.

6.2. Desorption kinetics of ethylbenzene from carbon surfaces

In this section, the desorption kinetics of ethylbenzene from four pristine carbon surfaces: highly oriented pyrolytic graphite, single-wall carbon nanotube bundles, carbon nanofibers and colloidal graphite are presented. By analyzing the TD data using peak maximum and Falconer-Madix methods, the activation energies of desorption and pre-exponential frequency factors are determined [Falconer and Madix, 1977; Redhead, 1962].

6.2.1. Temperature programmed desorption from carbon surfaces

A series of temperature calibrated TD spectra are obtained (Fig. 6.3) after exposing HOPG to a typical dose of up to 30 L of ethylbenzene (99.99 %, Aldrich). The exposure is carried out by admitting ethylbenzene vapors to a freshly cleaved graphite sample, maintained at 30 K, under ultrahigh-vacuum (UHV) conditions. The TD spectra are obtained by a constant heating rate of $2\,\mathrm{K\,s^{-1}}$. In general, they are characterized by a high temperature desorption feature due to the desorption from the first monolayer, with a corresponding peak maximum appearing at 210 K. For coverages greater than 1 ML, TD spectra also display a distinct low temperature shoulder at 175 K and a main peak centered around 170 K, which is due to the desorption from the second monolayer and multilayers, respectively. In the sub-monolayer region, the peak maximum T_{max} is independent of the initial surface coverage as indicated by a shift of only 2–3 K. Together with the shape of the TD spectra, this coverage independent peak maximum confirms a first-order desorption kinetics for sub-monolayer desorption of ethylbenzene from HOPG. The thermal desorption (TD) peaks due to the desorption from multilayers exhibit a common leading edge, characteristic of zero-order desorption kinetics, analogous to sublimation of solid ethylbenzene in equilibrium with its vapor. TD spectra from SWNT

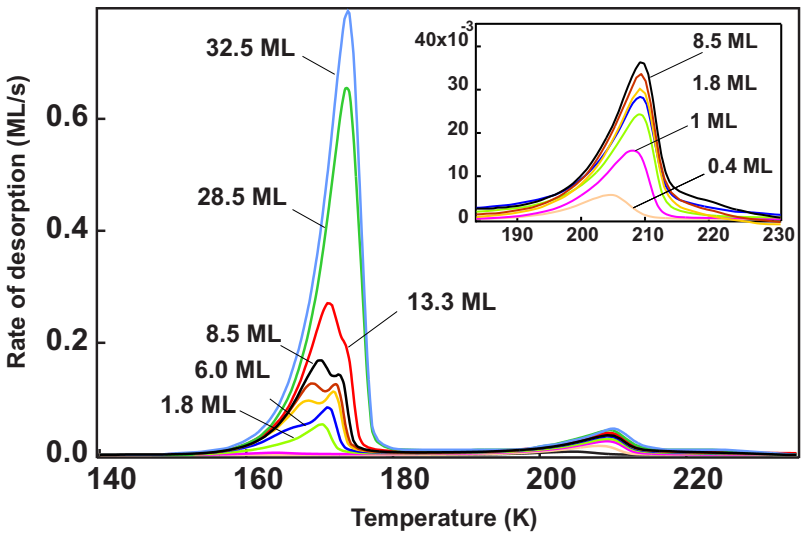

Figure 6.3.: Series of thermal desorption spectra of ethylbenzene from HOPG for gradually increasing surface coverage. The initial coverages are indicated in the graph in the units of close-packed monolayer of ethylbenzene on HOPG. In the inset, the expanded view of the desorption peak from sub-monolayer region is displayed. The heating rate used for recording the TD spectra is $2\,\mathrm{K\,s^{-1}}$.

bundles (Fig. 6.4) are obtained by exposing ethylbenzene vapors to a film of carbon nanotubes or bucky paper, which is prepared from a commercial aqueous suspension of single-wall carbon nanotubes (more details of the sample preparation can

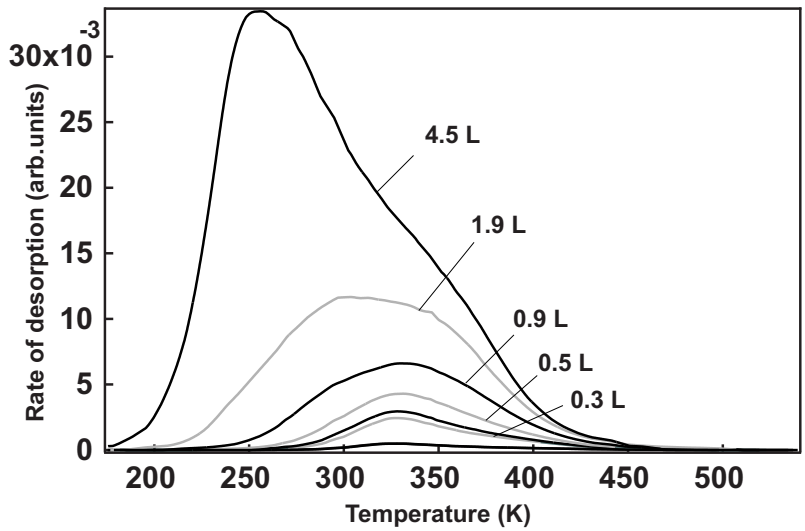

Figure 6.4.: Series of TD spectra of ethylbenzene obtained from SWNT bundles after exposing the sample surface up to a coverage of 4.5 L. The heating rate for the desorption is $1.25\,\mathrm{K\,s^{-1}}$.

be found in chapter 3). For outgassing this thin film or bucky-paper, it is affixed on a tantalum disk and cleaned by repeated annealing at 1100 K. The TD series of ethylbenzene from SWNT bundles are recorded by heating the sample at a constant rate of $1.25\,\mathrm{K\,s^{-1}}$ after exposing the surface to coverages up to 4.5 L.

In contrast to the sharp desorption features from HOPG, the TD spectra from nanotube bundles are relatively broad; the peak is broadened by ~ 50 K. Unlike the desorption traces from HOPG, there is no separation of mono- and multilayer peaks.

The TD traces at lower coverages (up to an exposure of 1 L) are symmetric, and have the peak maximum appearing between 300 and 350 K. The temperature corresponding to maximum desorption rate T_{max}, is found to be independent of initial coverages up to 0.9 L. However, after the saturation coverage corresponding to HOPG, the T_{max} shifts slowly to lower temperatures with increasing coverage. At higher coverages (4.5 L), the TD traces becomes even more asymmetric, displaying a peak-like structure at around 250 K, which grows further with coverage.

The broadening of the thermal desorption spectra of adsorbates from porous carbon surfaces is shown to be caused by three factors: (1) the diffusion of gases inside the porous materials which slows down the desorption kinetics (2) inhomogeneity of the sample surface due to defects and vacancies and (3) inhomogeneities from the presence of impurities such as transition metal catalysts [Hertel, 2003]. For bucky paper samples, the diffusion processes is found to be the dominant factor that broadens the desorption spectra. A comparison of the density of the samples used in these experiments with that of SWNT ropes indicates that the SWNT-samples used in our

experiments are 60 % void space [Hertel, 2003; Ulbricht et al., 2002a]. Due to this high porosity (with a typical specific surface area of $140\,m^2\,g^{-1}$), and also due to a higher co-ordination, the adsorbing molecules tend to preferentially occupy internal void spaces in SWNT bundles.

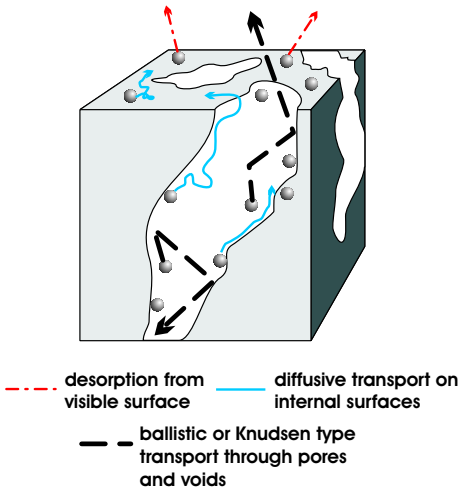

Figure 6.5.: Schematic illustration of three modes of transport: ballistic transport, diffusion and desorption, in a porous structure.

This preferential adsorption within the inner void regions is evident from the absence of any saturation even after the prolonged exposure of the SWNT surface to adsorbate quantities comparable to that on HOPG. Hence, during the desorption, surface concentration of the adsorbent is constantly replenished by the diffusion from the void spaces in the bulk to the surface. Therefore, when the thermal desorption of adsorbates from the porous sample surfaces is studied, the concentration profile of the adsorbates has to be accounted for the simultaneous diffusion processes (see the schematic illustration in Fig. 6.5). This coupled diffusion-desorption (CDD) model has shown that the diffusion within the pores or void regions inside the sample slow down the desorption kinetics and therefore leads to the broadening of the desorption peaks. Details of this coupled diffusion-desorption model are provided in chapter 2. In addition to this contribution from diffusion processes, the surface inhomogeneities such as vacancies or kinks, and presence of impurities also contribute to the desorption peak broadening.

A high coverage or saturation experiment where the SWNT bundles are exposed to doses of ethylbenzene typically 1000 times that on HOPG surface is performed to study the multilayer desorption features. Figure 6.6 display the series of TD spectra of ethylbenzene from SWNT bundles after the surface is exposed to adsorbate concentration equivalent to a coverage of 1270 ML on graphite. In order to compare the multilayer features obtained from SWNT samples with that from HOPG, the latter (green trace) is scaled by a factor of 100 and is displayed in the figure. It is found that SWNT bundles show the multilayer desorption feature when exposed to gas quantities above 960 ML, which shifts to lower temperatures with increasing coverage and finally converges to the multilayer desorption feature from graphite. The reason for this delayed appearance of multilayer features from SWNT bundles is the preferential adsorption of molecules within the high binding inner sites within the sample and takes place only after the saturation of the interior sites. That means, the type of adsorption on the HOPG and SWNT-bundles is similar except

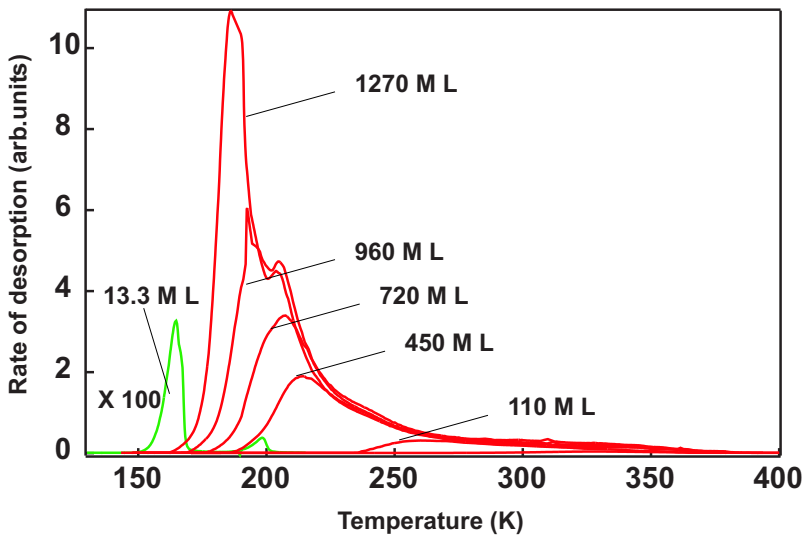

Figure 6.6.: High coverage TD spectra (red traces) of ethylbenzene desorption from SWNT bundles after exposing the sample surface to a coverage of ∼1000 ML. At this coverage regime, a saturation desorption feature similar to the multilayer desorption of ethylbenzene from graphite (green trace) is observed. The multilayer desorption spectrum from graphite is scaled down by a factor of 100. The heating rate for the desorption experiment was $0.25\,\mathrm{K\,s^{-1}}$.

that in the highly porous material, the appearance of multilayer peaks is delayed until the surface is exposed with very high dosage of typically around 1000 times

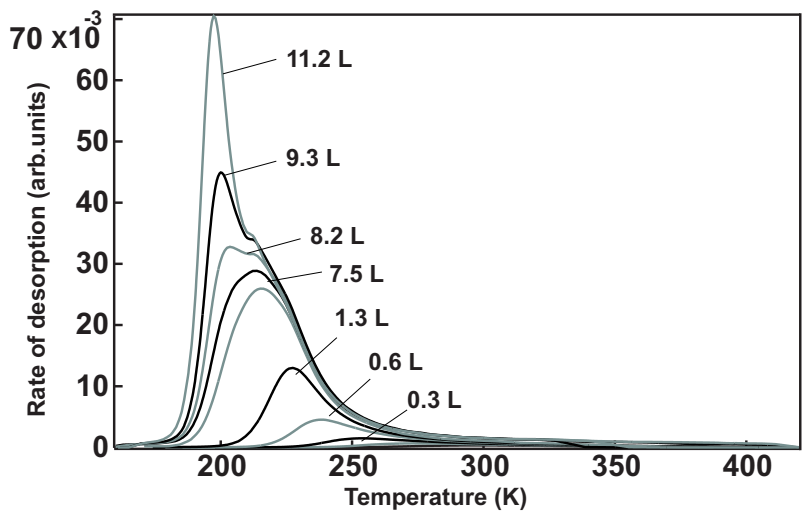

Figure 6.7.: Series of thermal desorption spectra of ethylbenzene from carbon nanofibers after exposing the surface up to a coverage of 11.2 L. The spectra are recorded with a heating rate of $1\,\mathrm{K\,s^{-1}}$.

that needed to form a close-packed monolayer on the graphite surface.

Thermal desorption spectra from carbon nanofibers (Fig. 6.7) and colloidal graphite (Fig. 6.8) after exposing the films of carbon nanofibers to coverages up to 11.2 L are recorded by a sample heating rate of 1 K s^{-1}. TD spectra from nanofibers exhibit desorption features very similar to those from carbon nanotubes (Fig. 6.4). However, the peaks are less broad at similar exposures, for example at $\sim$1 L. The onset of desorption appears at 190 K and the desorption tail extends up to 310 K, thus having a spread of 120 K. This is roughly 45 % less than the spread of the TD trace from nanotubes. At lower coverages, T_{max} appears around 250 K, which systematically shifts to lower temperature with an increase in coverage. At higher coverages a shoulder appears in the TD trace at 210 K, which continues to grow with the greater coverages. This shoulder corresponds to the desorption from multilayers. TD traces also exhibit a common leading edge at coverages higher than 8 L. The appearance of the multilayer peak (with an exposure of 7.5 L in Fig. 6.7) at a low coverage when compared to that from the SWNT bundles, indicates that the samples used here have lesser porosity. Figure 6.8 shows the thermal desorption

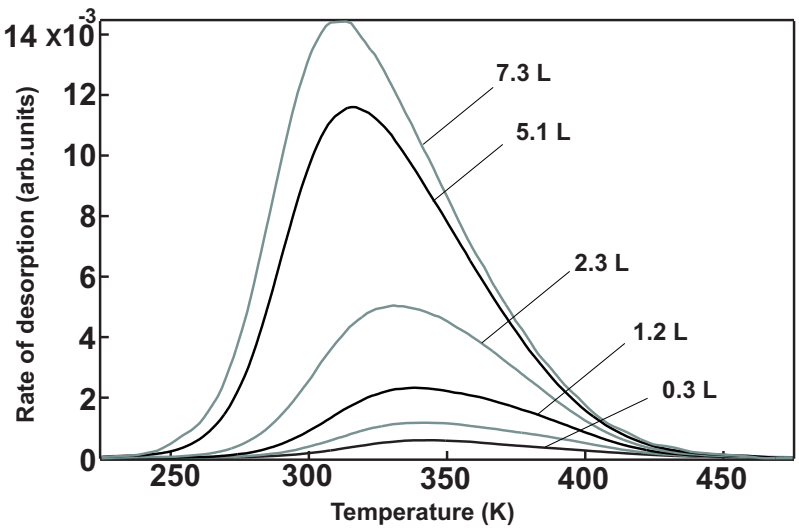

Figure 6.8.: Series of thermal desorption spectra of ethylbenzene from colloidal graphite after exposing the surface progressively up to a coverage of 7.3 L. The spectra are recorded using a heating rate of 1 K s^{-1}.

spectra from the colloidal graphite surface, exposed to a coverage of up to 7.3 L. The peak maximum is centered around 325 K for sub-monolayer coverages (i.e., less than 1.2 L) and shifts to around 315 K when the coverage is increased to 5.1 L. TD spectra from the colloidal graphite are characterized by the absence of a common leading edge and the feature that indicates the multilayer formation. The spectra are similar to that from the low coverage series from SWNT bundles, the broadening arising mainly due to the inhomogeneities present in the material.

6.2.2. Activation energy and pre-exponential factors

To determine the activation energy of desorption and pre-exponential frequency factors, the analysis of TD spectra is carried out using the Falconer-Madix (FM) method and also independently using the Redhead method (both are presented in chapter 3 in detail) [Falconer and Madix, 1977; Redhead, 1962]. Evaluation of TD spectra using the FM method is based on plots of the *logarithm of desorption rate* versus *logarithm of surface coverage*, at a constant temperature, i.e, under isothermal conditions. From the slope and the intercepts of the linear fits to these so called isothermal plots, the order of desorption (n), the frequency factor (ν) and the activation energy (E_d) can be obtained. The analysis is based on the following relation:

$$\ln\left(-\frac{d\theta}{dt}\right) = \ln(\nu) + n\ln(\theta) - \frac{E_d}{k_B T}. \tag{6.9}$$

Figure 6.9 displays typical isotherms obtained using TD spectra from HOPG in a temperature range of 193 and 197 K. From the slope of the linear fits to isotherms,

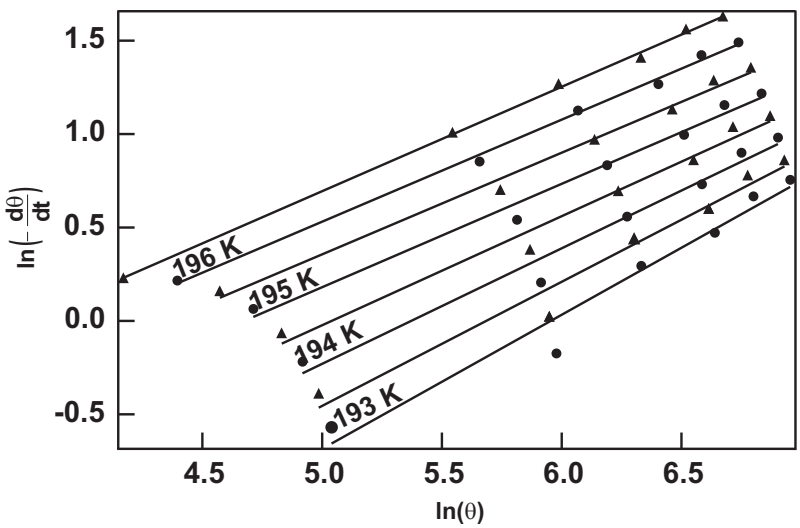

Figure 6.9.: Isotherms constructed from the thermal desorption of ethylbenzene from HOPG in the temperature range 193 K and 197 K, together with the straight line fits to the isotherms. Traces corresponding only to the sub-monolayer are used for the construction of the isotherms.

the order of counterpart desorption ($n = 0.91 \pm 0.15$) is obtained. This value, close to unity implies the first-order desorption kinetics of ethylbenzene desorption, which consistent with the observations of the temperature independent peak maximum and the shape of TD spectra. In order to calculate the activation energy and pre-exponential frequency factor, the y-intercepts (I) of the linear fits (obtained from

isothermal plots) are plotted versus $1/T$ [Fig. 6.10(a)], using the relation

$$I = \ln(\nu) - \left(\frac{E_d}{k_B T}\right), \tag{6.10}$$

the pre-exponential frequency factor ($5.1 \times 10^{14\pm0.1}\,\mathrm{s}^{-1}$) and the activation energy of desorption ($0.68 \pm 0.01\,\mathrm{eV}$) are obtained from the intercept and the slope, respectively. In a similar fashion, the isotherms for the desorption from SWNT bundles

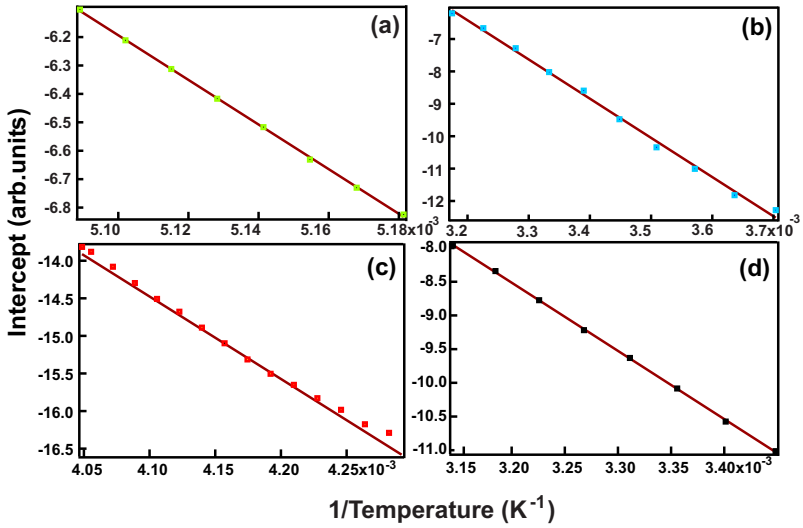

Figure 6.10.: Intercept plots (I versus $1/T$) for the ethylbenzene desorption from (a) HOPG, (b) SWNT-bundles, (c) nanofibers and (d) colloidal graphite and corresponding straight line fits.

are constructed for the temperature range of 270 and 320 K. The desorption from SWNT bundles also follows first-order kinetics as indicated by the slope of the isotherms ($n = 1.08 \pm 0.05$). However, this slope is found to deviate to about $n = 1.78 \pm 0.05$ at higher temperatures (270 K). Due to a commonly observed asymptotic divergence of diffusion rates with temperature ($\mathrm{rate}_{\mathrm{diff}} \propto \sqrt[3]{T}$), the representation of desorption kinetics (i.e., first-order desorption) is more accurate at lower temperatures [Reif, 1985]. Using the intercept plot [Fig. 6.10(b)], the activation energy and the pre-exponential frequency factor are calculated ($1.04 \pm 0.02\,\mathrm{eV}$ and $1.1 \times 10^{14\pm0.4}\,\mathrm{s}^{-1}$). Likewise, isotherms and intercept plots [Figs. 6.10(c) and (d)] are obtained for nanofibers and colloidal graphite. Corresponding activation energies and pre-exponential factors are hence determined (Table 6.1). The activation energies obtained using the FM method are confirmed by a subsequent calculation using the Redhead method [Redhead, 1962].

The Redhead method relates activation energy with frequency factor (ν), heating rate (β) and peak maximum as:

$$E_d = k_B T_{max}[\ln(\nu T_{max}/\beta) - 3.64]. \tag{6.11}$$

The application of the Redhead method as shown by the above equation, relies upon the availability of an accurate frequency factor (ν) and a clearly defined peak maximum (T_{max}) in the TD spectra. Conventionally, for simpler molecules, frequency factors for desorption are assumed to be in the range of 10^{12} to $10^{15}\,\mathrm{s}^{-1}$. Small errors of one or two orders of magnitude within this assumption induce only negligible error in the calculated activation energies [Christmann, 1991; Paserba and Gellman, 2001b; Zacharia et al., 2004]. Therefore, pre-exponential frequency factors obtained from the FM method can be used to determine the activation energies. Table 6.1 shows the activation energies of desorption from all carbon surfaces determined using the Redhead method and FM methods.

Table 6.1.: Activation energy and pre-exponential frequency factor for ethylbenzene desorption from graphite, nanotubes, nanofibers and colloidal graphite–comparison between the Falconer-Madix and the Redhead methods.

	Falconer–Madix		Redhead
	$\nu(\mathrm{s}^{-1})$	E_d(eV)	E_d(eV)
HOPG	$5.1\times10^{14\pm0.1}$	0.68±0.01	0.63±0.01
Nanotubes	$1.1\times10^{14\pm0.4}$	1.04±0.02	0.96±0.02
Nanofibers	$1.6\times10^{13\pm0.4}$	0.94±0.02	0.75±0.05
Colloidal graphite	$2.4\times10^{13\pm0.1}$	0.87±0.01	0.89±0.11

Within the experimental errors, the activation energy values obtained using the Redhead method are consistent with the values obtained using the FM method. Ambiguity in the exact monolayer coverage as well as a poorly defined peak maximum (T_{max}) in TD spectra for porous materials are reflected in larger uncertainties when the Redhead method is used. The activation energy for ethylbenzene desorption has a values typically in the range for the physisorption, which implies that the molecules are held on the surface by weak van der Waals interaction [Vidali et al., 1991]. Activation energies of desorption from porous carbon surfaces are nearly 25–50 % greater compared to that its planar graphene counterpart. This can be attributed to effective co-ordination, either in a groove site or in inner void regions in nanotube bundles or by the edge planes in the case of carbon nanofibers and colloidal graphite [Ulbricht et al., 2002a].

6.3. Desorption kinetics of ethylbenzene from oxidized carbon surfaces

As pointed out in the beginning of this chapter, oxidative dehydrogenation of ethylbenzene is the archetypal example for the catalytic performance of carbon surfaces.

This reaction is brought about by the adsorption of both ethylbenzene and oxygen molecules on the carbon surface, which undergo bimolecular surface reaction to form styrene. The catalytic performance of any surface for oxidation is attributed to the activation of either the hydrocarbon or the oxygen molecule, the latter by the formation of reactive oxygen species such as O^-, O^{2-} etc. [Bielański and Haber, 1991].

On carbon surfaces, these reactive species are formed by the reduction of an adsorbed O_2 molecule from π-electrons on graphitic basal planes. Such species, once formed, can be stabilized by the migration to reactive edge planes or defects (E in Fig. 6.11) where they can be covalently linked to the carbon surface [Maximova, 2002; Sanchez-Cortezon, 2002]. These covalently bonded oxygen atoms are frequently identified as polyfunctional groups analogous to those found in traditional organic chemistry and are observed to quantitatively enhance catalytic performance of carbon surfaces [Fabish and Schleifer, 1984; Maximova, 2002; Neffe, 1987; Pereira et al., 1999; Szymański et al., 2002]. The catalytic activity of the pristine carbon surfaces for ODH reaction has been found to be poor, and oxidation of the carbon is therefore a prerequisite for the ODH reaction on carbon surfaces.

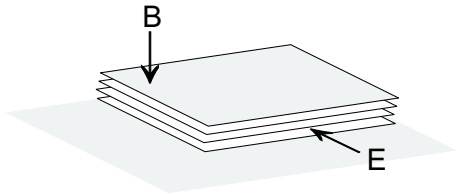

Figure 6.11.: Schematic representation of reactive edge (E) and basal (B) planes of graphitic layers.

This section presents the study of catalytic oxidative dehydrogenation of ethylbenzene. This is performed by exposing the oxidized carbon surfaces to ethylbenzene and monitoring the desorption of both ethylbenzene and styrene. Due to higher defect and edge plane densities, and a higher surface heterogeneity, carbon nanofibers and colloidal graphite are found to be most suitable surfaces for an oxidative dehydrogenation reaction (see chapter 3 for a discussion on structure of carbon nanofibers and carbon nanotubes) [Maximova, 2002]. Hence, the catalytic study presented here is limited to these two surfaces. The catalytic analysis, i.e., the evaluation of percentage conversion and selectivity, is based on the determination of surface concentrations of ethylbenzene and styrene from TD spectra. In order to obtain the exact surface coverages of styrene and ethylbenzene, the change in surface concentrations due to all kinetic processes, i.e., the bimolecular reaction and desorption are considered within the framework of the LH reaction mechanism.

6.3.1. Temperature programmed desorption from oxidized carbon surfaces

As pointed out in the beginning of this chapter, oxidative dehydrogenation of ethylbenzene on oxidized carbon surfaces leads to the formation of styrene and water. In a typical oxidative dehydrogenation experiment, the desorption of the reactant ethylbenzene and product styrene are generally detected by monitoring the signals

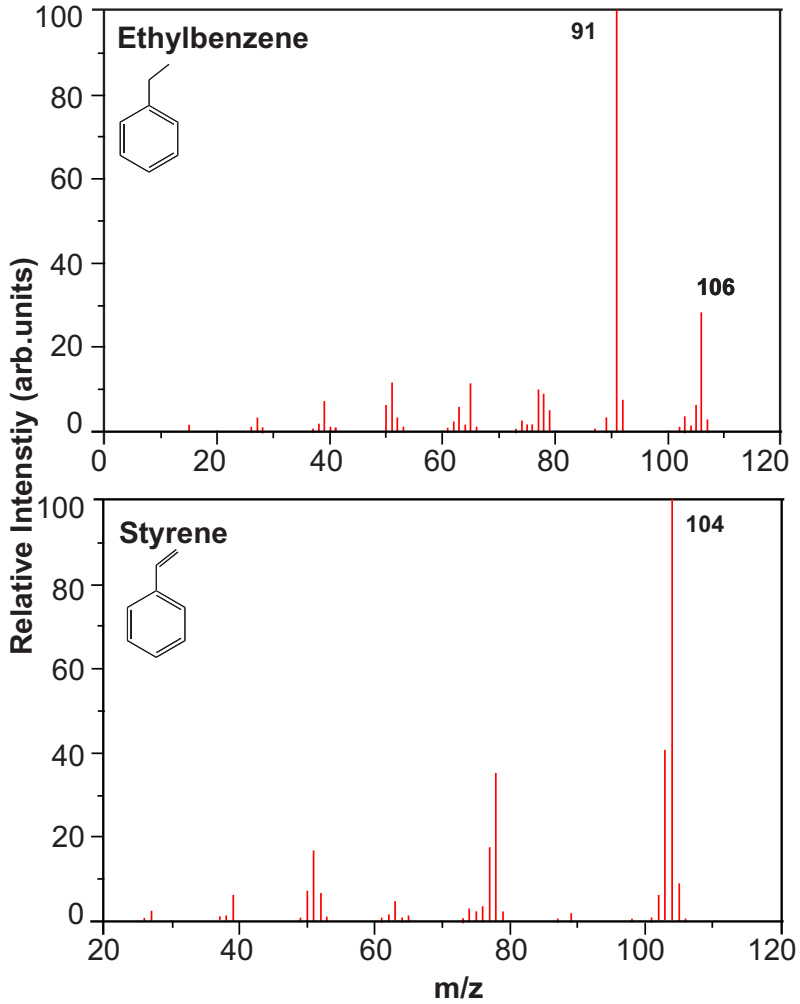

Figure 6.12.: Mass spectra of ethylbenzene (top panel) and styrene (bottom panel) showing peaks corresponding to different fragments. Desorption of ethylbenzene is monitored by tuning quadrepole mass spectrometer to m/e = 91 a.m.u/e and styrene to 104.

corresponding to their respective parent masses (i.e., m/e = 106 and 104 a.m.u/e). However, the relative intensity of the parent peak for ethylbenzene ($C_8H_{10}^+$) is weak (27:1.3) when compared to the same from peak fragment $C_7H_7^+$, i.e., m/e = 91 a.m.u/e (i.e., 100:1.3) [see cracking pattern of ethylbenzene and styrene in Fig. 6.12]. This is crucial when the simultaneous desorption of both styrene and ethylbenzene are monitored, as smaller quantities of styrene can be formed at quadrepole mass spectrometer (QMS) itself which do not originate from the catalytic conversion on surface. Thus, when the thermal desorption of ethylbenzene and styrene are simultaneously monitored, QMS is tuned to record mass-to-charge

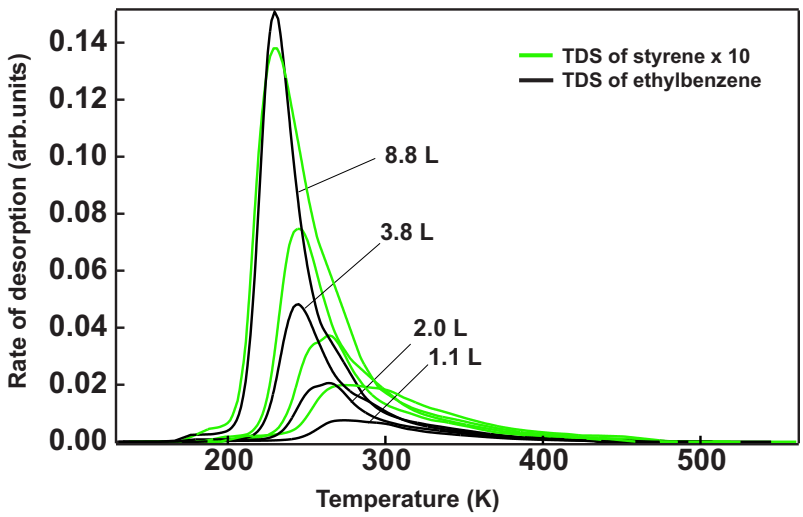

Figure 6.13.: Series of thermal desorption spectra of ethylbenzene (black trace) and styrene (green trace) from oxidized carbon nanofibers after the exposure of the sample surface with a dosage of up to 8.8 L of ethylbenzene. The traces corresponding to the desorption from styrene are scaled up by a factor of 10 for comparison. The mass spectra corresponding to the ethylbenzene and styrene are recorded by tuning the QMS to mass-to-charge ratios 91 and 104 a.m.u./e. The heating rate used is $1\,\mathrm{K\,s^{-1}}$.

ratio of 91 and 104 a.m.u./e. A series of coverages of ethylbenzene, up to 8.8 L and 2 L is obtained by exposing the oxidized carbon nanofibers and colloidal graphite surfaces, respectively, with ethylbenzene vapor. Prior to dosing with ethylbenzene, both carbon nanofibers and colloidal graphite are oxidized using H_2O_2 (60 % by vol.) under mild oxidation conditions (see chapter 5 for oxidation conditions).

Figures 6.13 and 6.14 show the TD spectra of ethylbenzene and styrene obtained using a heating rate of $1\,\mathrm{K\,s^{-1}}$ from carbon nanofibers and colloidal graphite, respectively. The shape and the position of TD traces of ethylbenzene desorption traces after oxidation are similar to those seen before oxidation (i.e., Figs. 6.7 and 6.8). Absence of quantifiable differences after oxidation can be attributed to highly inhomogeneous as well as rough surfaces. In order to determine activation energy and frequency factor, both isothermal analysis and Redhead analysis are performed. Using the intercepts (I) from isotherms, plots of I versus 1/Temperature (Fig. 6.15) are constructed. Pre-exponential frequency factors and activation energies are calculated using the slope and intercept of the linear fits of plots in Fig. 6.15. The calculated value of pre-exponential frequency factors and activation energies for the desorption of ethylbenzene and styrene are displayed in Table 6.2.

The binding energies of the educt (ethylbenzene) and that of the product (styrene) suggest that they are held on the oxidized carbon surface by physisorption forces. The reaction between physisorbed ethylbenzene molecule and carbon-oxygen sur-

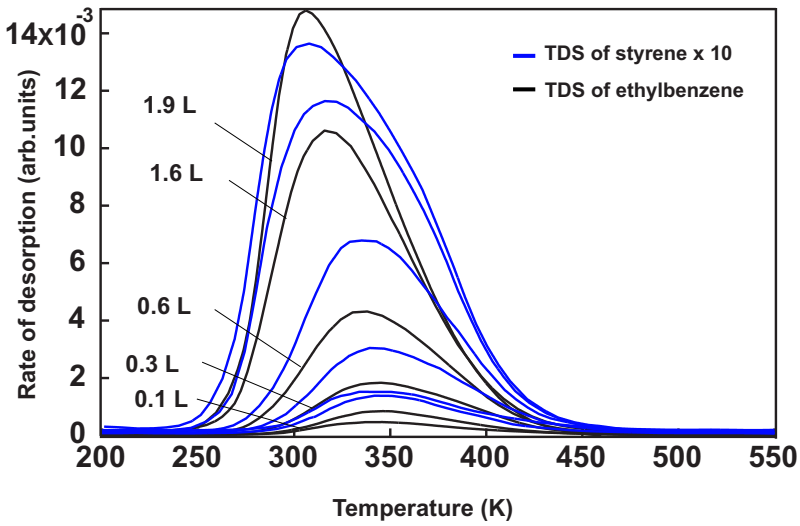

Figure 6.14.: Series of thermal desorption spectra of ethylbenzene (black trace) and styrene (blue trace) from oxidized colloidal graphite after the sample surface is exposed to a dosage of up to 1.9 L of ethylbenzene. The traces corresponding to the desorption from the styrene are scaled up by a factor of 10 for comparison. The mass spectra corresponding to the ethylbenzene and styrene are recorded by tuning the QMS to mass-to-charge ratios 91 and 104 a.m.u./e. The heating rate used is $1\,\mathrm{K\,s^{-1}}$

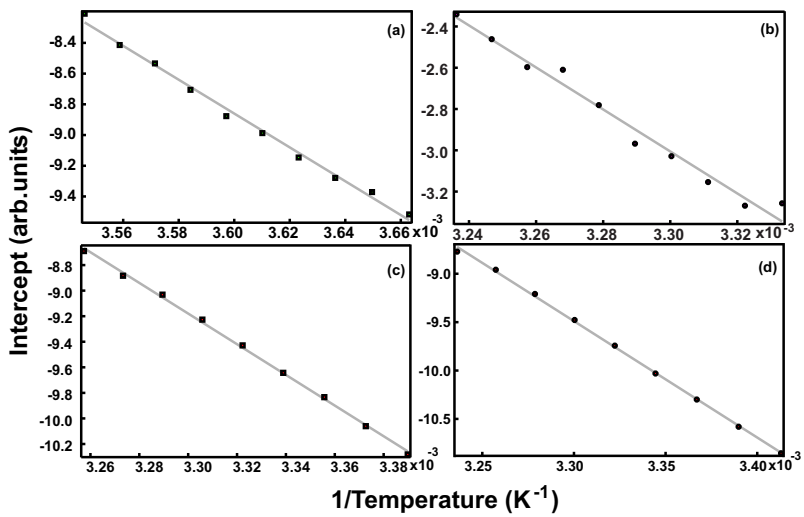

Figure 6.15.: Intercept plots (I versus $1/T$) constructed from the isotherms corresponding to the desorption of (a) ethylbenzene and (b) styrene from oxidized carbon nanofibers and (c) ethylbenzene and (d) styrene from oxidized colloidal graphite.

face functional group can be understood by comparing them to the mechanism of

Table 6.2.: Activation energies and pre-exponential frequency factors for ethylbenzene and styrene desorption from oxidized carbon nanofibers and colloidal graphite surfaces–comparison between the Falconer–Madix and the Redhead methods.

Gases and surfaces	Falconer–Madix		Redhead
	$\nu(\mathrm{s}^{-1})$	E_a(eV)	E_a(eV)
Ethylbenzene from CNF	$2.4\times10^{13\pm0.5}$	0.95±0.03	0.85±0.08
Styrene from CNF	$1.9\times10^{13\pm0.8}$	0.88±0.05	0.76±0.08
Ethylbenzene from CG	$1.6\times10^{13\pm0.2}$	1.03±0.02	0.95±0.02
Styrene from CG	$1.3\times10^{13\pm0.2}$	1.04±0.01	0.96±0.02

oxidative dehydrogenation reaction in traditional organic chemistry. Amongst various carbon-oxygen surface groups presented in the chapter 5, I consider the reaction between a quinone functionality and ethylbenzene. The justification for considering this surface groups is that the oxidation of graphene sheet can be likened to the oxidation of polyaromatic hydrocarbon molecules, which are known to produce quinone functional groups [*1,4*-quinonoid functional group, see Fig. 6.16(3)] [March, 1985]. In addition, quinones are typically used as oxidants and dehydrogenation agents in organic chemistry reactions when compared to other functionalities such as carboxylic acid or anhydride [Becker, 1974; March, 1985]. Formation of this func-

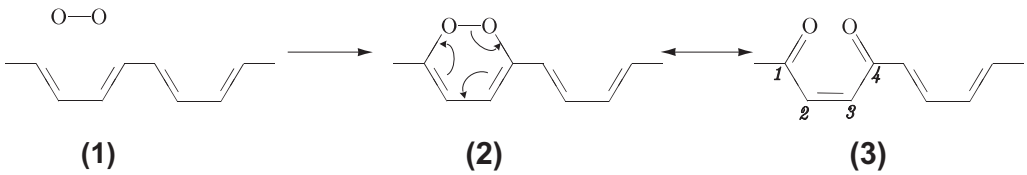

Figure 6.16.: Formation of a quinonoid surface functional groups is envisaged as the result of the chemisorption of molecular oxygen on the armchair edge of the graphene sheet (for details, see the oxidation of carbon surfaces in chapter 5). The chemisorption leads to the formation of aromatic peroxide (2) which rearranges to form the *1,4*-quinoid functional group (3). The curved arrows in step 2 indicates the direction of electron transfer.

tional group is depicted in Fig. 6.16. The reaction is initiated by the chemisorption of molecular oxygen on the top edge site of a graphene armchair edge, which is indicated by step 1 in Fig. 6.16 [Zhu et al., 2000]. The chemisorption leads to in the formation of an aromatic peroxide-type functional group (step 2). This aromatic peroxide undergoes an electron rearrangement, as indicated in the step 3, and leads to the formation of *1,4*-quinonoid functional group [Gleicher, 1974].

To understand the mechanism of the ethylbenzene ODH reaction on the oxidized

carbon surfaces, the interaction of the above *1,4*-quinonoid functional group with a physisorbed ethylbenzene molecule is considered (Fig. 6.17), and is compared with the traditional organic chemistry reaction mechanism [Braude et al., 1960; Trost, 1967]. The first step (1) of this reaction is the transfer of a hydride (H^-) from the ethylbenzene to the surface functional group. This reaction results in the formation of an ethylbenzene carbocation and a phenolate ion (shown in step 2). In the second step, the phenolate ion abstracts a proton (H^+) from the carbocation, which leads to the formation of styrene and a hydroquinone surface group. Reactions involving

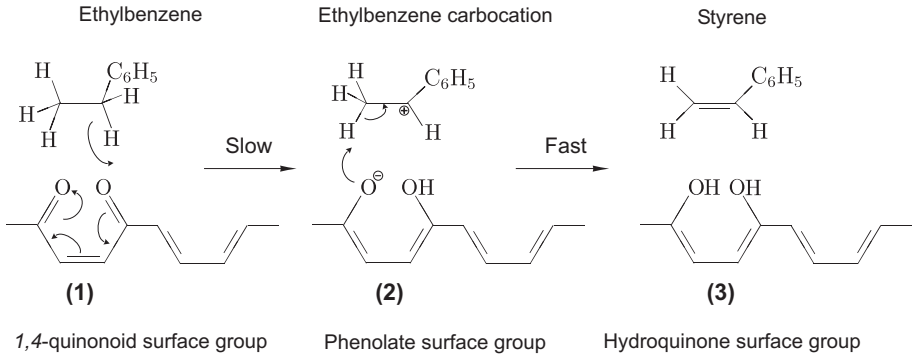

Figure 6.17.: First step (1) of the reaction involves the transfer of a hydride ion (H^-) from the ethylbenzene to the oxygen of *1,4*-quinonoid functional group. This results in the formation of an ethylbenzene carbocation and a phenolate ion, which are indicated in (2). Next step involves the transfer of a proton (H^+) from the ethylbenzene carbocation to the phenolate ion resulting in the formation of the styrene and hydroquinone [shown in (3)]. The curved arrows in (1) and (2) indicate the direction of the electron transfer.

quinones and alkyl substituted aromatic hydrocarbons are found to be assisted by the stability of the carbocation that is formed in the step (2) [March, 1985]. Its stability is due to the delocalization of the positive charge, and for the ethylbenzene carbocation this stabilization is shown in Fig. 6.18. For the dehydrogenation

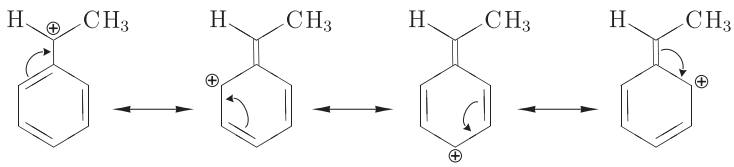

Figure 6.18.: Resonance stabilization of the ethylbenzene carbocation by the delocalization of positive charge over the aromatic ring.

of molecules similar to ethylbenzene, reaction rate studies have proposed that the elimination of a proton by the carbocation, as indicated by the step 2, is the fastest step [March, 1985]. The bimolecular reaction between ethylbenzene and the quinone functional group is the slowest and rate determining step [March, 1985].

6.3.2. Analysis of catalytic activity of carbon substrates

Conventionally, catalytic performance of a surface in heterogeneous catalysis is expressed in terms of percentage conversion of a reactant, or more precisely, in terms of the selectivity to form the product of interest [Campbell, 1988; Cornils et al., 2000]. For the oxidative dehydrogenation of ethylbenzene, the percentage conversion (C_{EB}) is defined as the ratio of concentration of ethylbenzene reacted to initial concentration:

$$C_{EB}\ (\%) = \frac{[EB]_i - [EB]_o}{[EB]_i} \times 100, \tag{6.12}$$

and the selectivity of styrene (S_{ST}) formation is given by the ratio of styrene formed to concentration of ethylbenzene reacted:

$$S_{ST}\ (\%) = \frac{[ST]_o}{[EB]_i - [EB]_o} \times 100, \tag{6.13}$$

where $[EB]_i$, $[EB]_o$ and $[ST]_o$ are concentrations of ethylbenzene and styrene before and after ODH reaction. As discussed below, these parameters can be expressed in terms of transient surface and gas phase concentrations of ethylbenzene and styrene, which can directly be obtained by integrating TD traces.

If $[EB]_{s,T_1}$ and $[EB]_{s,T_2}$ are the surface concentrations of ethylbenzene at two different temperatures T_1 and T_2 ($T_2 > T_1$), then, the concentration of ethylbenzene that disappeared from the surface between this temperature range can be represented as the sum of ethylbenzene in the gas phase at T_2 (due to desorption) and concentration of ethylbenzene that has undergone reaction:

$$[EB]_{s,T_1} - [EB]_{s,T_2} = [EB]_{g,T_2} + [EB]_{r,T_2}, \tag{6.14}$$

where $[EB]_{g,T_2}$ is the gas phase concentration of ethylbenzene and $[EB]_{r,T_2}$ is the concentration of ethylbenzene that has reacted at T_2. The gas phase concentration of ethylbenzene, $[EB]_{g,T_2}$ can be obtained in terms of the concentration of styrene, by rearranging the above equation, if we assume an equi-molar conversion of ethylbenzene to styrene. This assumption introduces only negligible error, as the concentrations of by-products such as toluene, benzene etc., are found to be insignificant even at higher temperatures ($< 4\,\%$) and it is generally applied for kinetic modeling studies of ODH [Pereira et al., 2000]. Therefore, Eq. (6.14) can be written as:

$$[EB]_{g,T_2} = [EB]_{s,T_1} - [EB]_{s,T_2} - [ST]_{s,T_1}. \tag{6.15}$$

The concentration of reacted ethylbenzene, $[EB]_i - [EB]_o$ is then, can be given by:

$$[EB]_i - [EB]_o = [EB]_{s,T_1} - [EB]_{s,T_1} - [ST]_{s,T_1} \tag{6.16}$$

$$= [ST]_{s,T_1}. \tag{6.17}$$

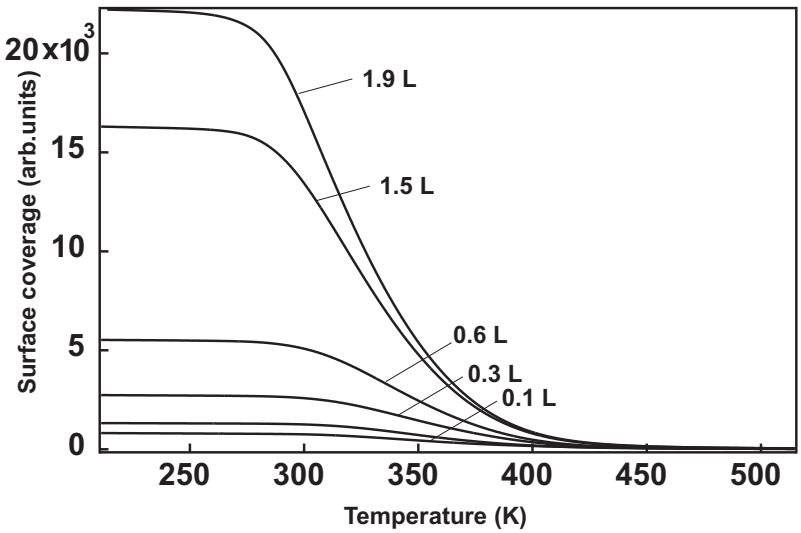

Figure 6.19.: The surface concentration of ethylbenzene $[EB]_s$ on colloidal graphite as a function of the temperature determined by integrating the thermal desorption traces. The exposures shown in the figure corresponds to various doses of ethylbenzene indicated in Fig. 6.14.

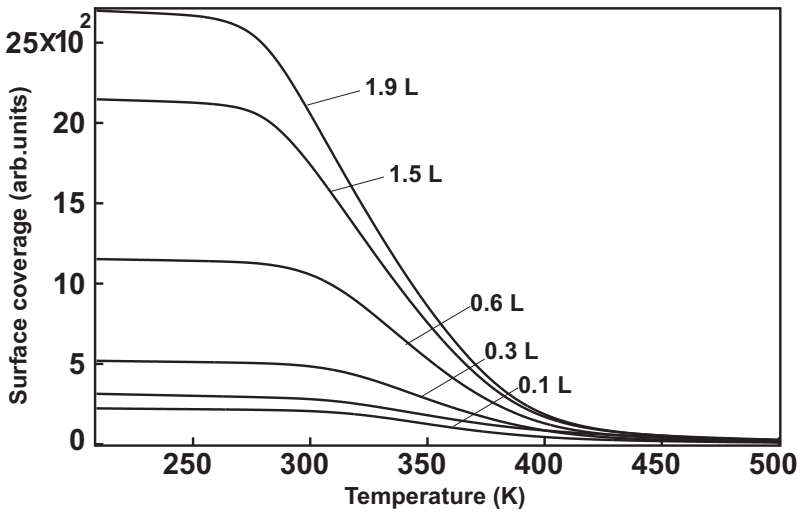

Figure 6.20.: The surface concentration of styrene $[ST]_s$ on colloidal graphite as a function of the temperature, determined by integrating the thermal desorption traces. The exposures correspond to the various doses of ethylbenzene indicated in Fig. 6.14.

Using the above equation, the percentage conversion of ethylbenzene is represented as:

$$C_{EB}\ (\%) = \frac{[\mathrm{ST}]_{\mathrm{s,T_1}}}{[\mathrm{EB}]_{\mathrm{s,T_1}}}, \tag{6.18}$$

and the selectivity of styrene formation between the temperature range T_1 and T_2 can be calculated using the following equation:

$$S_{ST}\ (\%) = \frac{[ST]_{s,T_1} - [ST]_{s,T_2}}{[ST]_{s,T_1}}. \tag{6.19}$$

The temperature dependence of surface coverage is evaluated by integrating TD spectra. The surface coverages of ethylbenzene and styrene on colloidal graphite are shown in Figs. 6.19 and 6.20. Similarly, the respective plots for carbon nanofibers

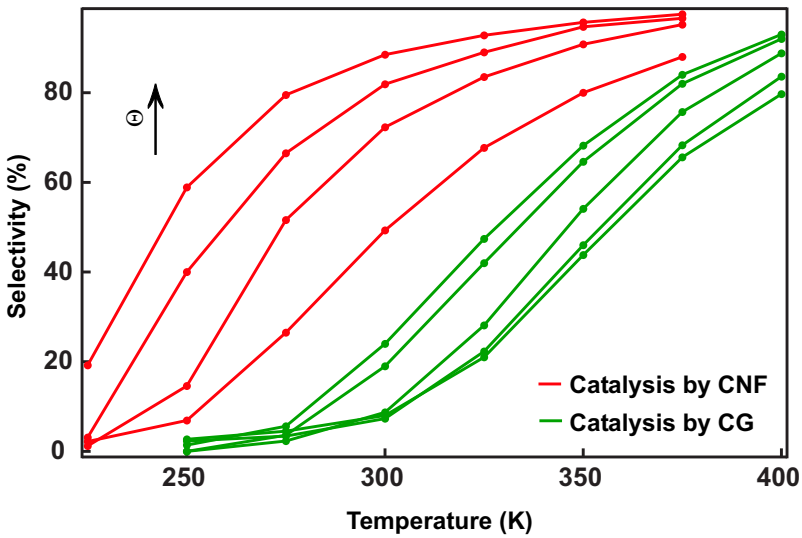

Figure 6.21.: Selectivity to form styrene (S_{ST}) by oxidative dehydrogenation as a function of temperature: catalysis by nanofibers (red traces) and colloidal graphite (green traces), for various initial coverages. The arrow points the direction of increase of surface concentration. Initial coverages on nanofibers are (8.8, 3.8, 2.0 and 1.1 L) and on colloidal graphite are (1.9, 1.5, 0.6, 0.3 and 0.1 L).

are also obtained by integrating the TD traces. The percentage conversion of ethylbenzene (C_{EB}) is evaluated from above equations and is found to be nearly 15 % at 220 K and increases to 25 % with the surface temperature. As the contribution from the homogeneous gas phase to the formation of styrene is reported to be only less than 2 %, even at elevated temperatures, the above increase in conversion can be attributed to the surface reaction [Maximova, 2002; Pereira et al., 1999]. This value, is considerably small when compared to nearly 65 % conversion observed in traditional catalytic experiments [Maximova, 2002]. This is due to a relatively low surface temperature in our experiments as compared to around 700–850 K in other common catalytic reactions. Additionally, the conversion rate is severely hampered in our experiments due to a high desorption rate. Figure 6.21 shows styrene selectivity as a function of surface temperatures, for various initial surface coverages of

ethylbenzene. Styrene selectivity clearly increases with temperature and reaches a constant value of around 93 % above 340 K. This higher selectivity when compared to standard catalytic experiments ($\sim$ 80 %), indicates that at surface reaction level, styrene production on carbon has proceeded nearly to completion. Selectivity as seen in the figure increases with the initial surface concentration, indicate the increased access of highly dense and reactive edge planes of nanofibers. The increase in surface concentration of styrene with the surface temperature clearly indicates that the reaction is catalyzed on the surface, rather than being produced by homogeneous gas phase reactions or by the cracking at mass spectrometer.

6.4. Summary and outlook

In the first part of this chapter, the desorption kinetics of ethylbenzene from four carbon surfaces: HOPG, SWNT-bundles, nanofibers and colloidal graphite were presented. The activation energies of desorption and pre-exponential frequency factors were calculated from the thermal desorption spectra using Falconer-Madix and Redhead methods. The activation energy of ethylbenzene on graphite is found to be 0.68 ± 0.01 eV, which is nearly 30–35 % smaller in comparison to binding energies on porous carbon structures (for instance, on SWNT bundles, activation energy is found to be 1.04 ± 0.02 eV). This significant increase in binding energies, and also the broadening of desorption peaks observed for single-wall carbon nanotube bundles, is attributed to the greater co-ordination of adsorbents and to their slower desorption kinetics. Both of these effects are caused by the preferential adsorption of gas molecules inside the interior porous volume of nanotube samples. However, desorption peak broadening in less porous carbon nanofibers and colloidal graphite arises from the greater defect density and the high inhomogeneity in those materials. By studying the desorption from SWNT bundles after exposure to doses of ethylbenzene exceeding coverage equivalents of 1000 close-packed monolayers on HOPG, it was shown that the adsorption on porous carbon surfaces arises due to same kind of interactions as that in planar HOPG surface.

The second part of this chapter was devoted to the determination of oxidized carbon surfaces' catalytic properties using oxidative dehydrogenation of ethylbenzene as a model reaction. For this experiment, oxidized carbon surfaces were exposed to ethylbenzene and subsequently the desorption of the educt (ethylbenzene) and the product (styrene) were monitored. Assuming a Langmuir-Hinshelwood type of kinetics for this reaction, their activation energies and pre-exponential factors for desorption were obtained from the TD spectra. The energetics of ethylbenzene desorption from an oxidized carbon surface are found to be similar to those from pristine carbon surfaces. A reaction mechanism involving physisorbed ethylbenzene molecules with surface functional groups is proposed by utilizing similar reaction mechanisms in traditional organic chemistry. By integrating the thermal desorption

spectra, the instantaneous surface coverage of the educt and product is determined. This data is used to evaluate the conversion percentage of ethylbenzene and the reaction selectivity. A very low percent converted of 15 % is observed at a temperature of 220 K, which increased to 25 % at around 400 K. The relatively low conversion observed in these thermal desorption experiments compared to nearly 65 % conversion recorded in traditional catalytic experiments, is primarily due to the low residence time of the educt on the surface. Additionally, the reaction temperatures used in the present experiments are considerably lower compared to typical catalytic experiments. Furthermore, low surface concentrations of reactive oxygen species, which are unknown quantities in our experiments, may lead to lower reaction yields. Selectivity of styrene formation is found to be higher (93 %) at temperatures above 340 K when compared to traditional catalytic experiments (80 %).